

Supramolecular Liquid Crystal Carbon Dots for

## Solvent-free Direct Ink Writing

*Yixuan Wang,<sup>a</sup> Yun Liu,<sup>b</sup> Xingtian Hao,<sup>a</sup> Xingping Zhou,<sup>a,c</sup> Haiyan Peng,<sup>\*,a,c</sup> Zhihao Shen,<sup>b</sup> Ivan I.*

*Smalyukh,<sup>d</sup> Xiaolin Xie,<sup>\*,a,c</sup> Bai Yang<sup>e,f</sup>*

Y. X. Wang, Dr. X. T. Hao

<sup>a</sup> Key Lab of Material Chemistry for Energy Conversion and Storage, Ministry of Education, and Hubei Key Lab of Materials Chemistry and Service Failure, School of Chemistry and Chemical Engineering, Huazhong University of Science and Technology (HUST), Wuhan 430074, China

Y. Liu, Prof. Z. H. Shen

<sup>b</sup> Beijing National Laboratory for Molecular Sciences, Key Laboratory of Polymer Chemistry and Physics of Ministry of Education, Center for Soft Matter Science and Engineering, College of Chemistry and Molecular Engineering, Peking University, Beijing 100871, China

Prof. X. P. Zhou, Prof. H. Y. Peng, Prof. X. L. Xie

<sup>a</sup> Key Lab of Material Chemistry for Energy Conversion and Storage, Ministry of Education, and Hubei Key Lab of Materials Chemistry and Service Failure, School of Chemistry and Chemical Engineering, Huazhong University of Science and Technology (HUST), <sup>c</sup> National Anti-Counterfeit Engineering Research Center, Wuhan 430074, China

This article has been accepted for publication and undergone full peer review but has not been through the copyediting, typesetting, pagination and proofreading process, which may lead to differences between this version and the [Version of Record](#). Please cite this article as [doi: 10.1002/adma.202303680](https://doi.org/10.1002/adma.202303680).

This article is protected by copyright. All rights reserved.

Prof. I. I. Smalyukh

<sup>d</sup> Department of Physics and Material Science and Engineering Program, University of Colorado at Boulder, Boulder, Colorado 80309, United States

Prof. B. Yang

<sup>e</sup> State Key Laboratory of Supramolecular Structure and Materials, College of Chemistry, Jilin University, <sup>f</sup> Optical Functional Theragnostic Joint Laboratory of Medicine and Chemistry, The First Hospital of Jilin University, Changchun 130012, China

\*Corresponding authors:

E-mail: hypeng@hust.edu.cn (H. Y. Peng); xlxie@hust.edu.cn (X. L. Xie)

This article is protected by copyright. All rights reserved.

**Abstract:** Recent years have witnessed the major advances of nanolights with extensive exploration of nano-luminescent materials like carbon dots (CDs). However, solvent-free processing of these materials remains a formidable challenge, impeding endeavors to develop advanced manufacturing techniques. Herein, in response to this challenge, liquid crystallization is demonstrated as a versatile and robust approach by deliberately anchoring flexible alkyl chains on the CDs surface. Alkyl chain grafting on the CDs surface is observed to substantially depress the common aggregation-caused quenching effect, and results in a shift of self-assembly structure from the crystalline phase to smectic liquid crystalline phase. The liquid crystalline phase transition temperature is ready to adjust by varying the alkyl chain length, endowing low temperature ( $< 50$  °C) melt-processing capabilities. Consequently, the first case of direct ink writing (DIW) with liquid crystal (LC) carbon dots is demonstrated, giving rise to highly emissive objects with blue, green and red color fluorescence, respectively. Another unexpected finding is that the DIW with LC inks dramatically outperforms the DIW with isotropic inks, further highlighting the significance of LC processing. The reported approach herein not only exhibits a fundamental advance by imparting LC functions to CDs, but also promises technological utility in DIW-based advanced manufacturing.

This article is protected by copyright. All rights reserved.

**Keywords:** nanolight, carbon dots, liquid crystals, direct ink writing, additive manufacturing

This article is protected by copyright. All rights reserved.

## 1. Introduction

Recent years have seen the major advances of nanolights for numerous applications ranging from flat-screen display to biological imaging.<sup>[1]</sup> These advances are accompanied by the significant increase of freedom in the design of nano-luminescent materials via dialing the chemical compositions other than tuning the nanoparticle size or shape. Enhanced freedom of design has led to the extensive exploration of new classes of highly emissive nano-luminescent materials such as AIEgens (i.e., aggregation induced emission luminogens) and carbon dots (CDs).<sup>[2]</sup>

Among all nano-luminescent materials, CDs have drawn particular attention from both organic and inorganic scientific communities as they can be synthesized via convenient methods with organic precursors and also present typical characteristics of inorganic nanoparticles.<sup>[3]</sup> The synthesis process is quite simple without the requirement of sophisticated method designs and tedious purification. In addition, due to the broad availability of organic precursors ranging from small molecules to high molecular weight polymers, both the CDs absorption and emission properties can be precisely tuned in a wide range of frequencies from ultraviolet (UV) to near-infrared (NIR).<sup>[4]</sup> Moreover, the emission type can be dialed from fluorescence to phosphorescence and even upconversion by carefully selecting the organic precursors.<sup>[5]</sup> Last but not least, CDs are usually less toxic and more

This article is protected by copyright. All rights reserved.

biocompatible than their counterparts for biochemical applications.<sup>[6]</sup> However, CDs typically yield very weak or even no emission in bulk compositions despite of the bright emission when nano-scale dispersed, which is known as the aggregation-caused quenching (ACQ) effect.<sup>[7]</sup> To tackle the ACQ issue, embedding CDs in a hydrophilic matrix such as poly(vinyl alcohol), sodium alginate and porous zeolites has been proven useful due to that the supramolecular hydrogen bonding interactions between CDs and the matrix can effectively constrain the CDs aggregation and prevent nonradiative relaxations.<sup>[5a,6c,7a,8]</sup> Unfortunately, lots of solvents are generally required to reshape (e.g., printing) these CDs-containing materials,<sup>[6c,8a,9]</sup> which would hamper endeavors to develop more efficient and environmentally friendly manufacturing techniques. Another exciting breakthrough to overcome ACQ has been recently achieved by Lu and co-workers through surface modification of CDs with salicylaldehyde-type or chlorosalicylaldehyde ligands.<sup>[4a,10]</sup> Supramolecular hydrogen bonding interactions inside and between these as-prepared CDs have also been found critical for provoking the emission properties by greatly constraining molecular motions. In these cases, however, the strong hydrogen bonding interactions between CDs also have a large possibility to prevent easy processing in the absence of solvent. Clearly, to meet the ever-increasing demands for advanced manufacturing toward high-tech applications, solvent-free processing of CDs is highly desirable but remains a formidable challenge.

This article is protected by copyright. All rights reserved.

Liquid crystal (LC) processing emerges as a powerful strategy in response to the above challenges. LC represents a class of soft matter in mesophase between fluidic isotropic liquids and solid anisotropic crystals, and it usually exhibits both liquid fluidity and anisotropy commonly associated with solid crystals.<sup>[11]</sup> Owing to the appealing capability of delivering programmed, reversible and rapid responses to external stimuli such as light and heat,<sup>[12]</sup> many LC materials have been developed as “smart” materials for a wide variety of promising applications ranging from electro-optic display to reprocessable hard vitrimers and robotic actuators.<sup>[13]</sup> Apart from the astonishing stimuli-responsivity, another important feature of LC materials is that they can enable facile processing due to the dramatically decreased internal friction and viscosity stemming from the long-range orientational ordering over a large range of scales. The most famous example of LC processing dates back to 1971 when poly(*p*-phenylene terephthalamide) was successfully made into Kevlar<sup>®</sup> fibers with ultrahigh strength and mechanical resilience. This success was achieved by DuPont and would not be possible without LC processing due to the strong confinement by inter-chain hydrogen bonding interactions. This major breakthrough has always inspired further innovations of LC processing. For instance, Wu and co-workers have developed a novel LC processing approach in 2017 with the discovery of photoswitching-induced reversible solid-to-liquid transition of azobenzene-containing polymers.<sup>[14]</sup> This approach has proven useful to create optical anticounterfeiting patterns with multiple security features.<sup>[15]</sup> Distinctly,

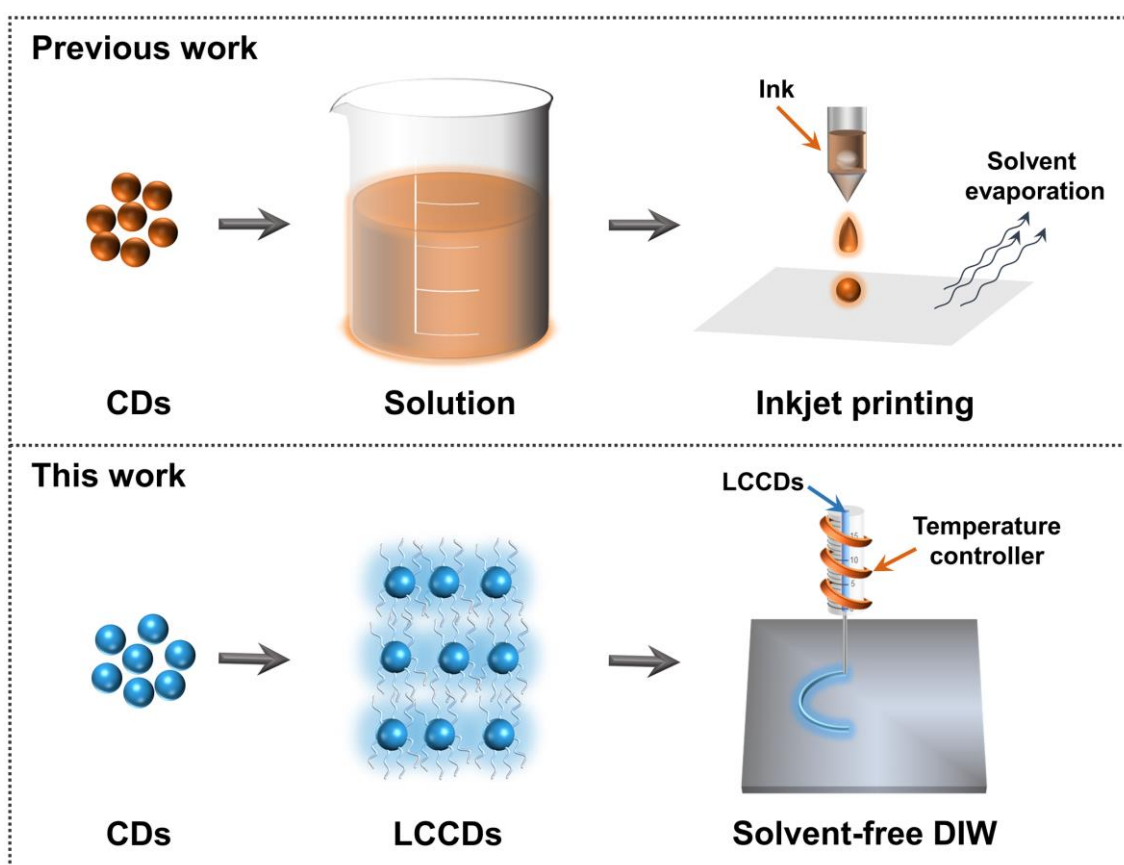
This article is protected by copyright. All rights reserved.

Schenning and co-workers have realized 4D printing of elastomer actuators using inks of LC polythiourethane.<sup>[16]</sup> However, LC processing of CDs-based materials has not been exploited to date due to the lack of toolbox to impart LC functions to CDs and the lack of fundamental understanding of the structure-property relationship for achieving predesigned LC properties.

Herein, building on the experiences to impart LC functions to zinc sulfide nanoparticles and supramolecular metallacycles,<sup>[11e,17]</sup> we present the first case of solvent-free processing of CDs via liquid crystallization by deliberately anchoring flexible alkyl chains on their surface. Distinct from previous strategy of utilizing hydrogen bonding interactions, weaker supramolecular van der Waals interactions were employed here which drove the shift of the self-assembled structure of CDs from the crystalline phase to the smectic LC phase. Bulk emissive LCCDs (i.e., the liquid crystal carbon dots) were yielded in three primary colors of red, green and blue, respectively, due to the prevented aggregation and limited ACQ. The phase transition behaviors of the resulting LCCDs were found highly dependent on the alkyl chain length, offering the opportunity to realize solvent-free processing under low temperatures. Eventually, direct ink writing (DIW) using the LCCDs inks was successfully realized (**Figure 1**), demonstrating a more efficient and environmentally friendly route to reshape CDs-based materials. DIW has emerged as the most versatile additive manufacturing technique based on extrusion of viscoelastic inks for printing 3D structures with intricate architectures and compositions at the meso- and microscale.<sup>[18]</sup> Therefore, DIW of LC

This article is protected by copyright. All rights reserved.

materials is highly promising for advanced manufacturing such as 3D and 4D printing because the LC molecular orientation and hierarchical structures can be well-controlled over a broad range of scales.<sup>[12b,18a,19]</sup> It is further worth noting that although Xie et al. have successfully tackled ACQ effect of yellow–green color emissive CDs by grafting mesogenic groups,<sup>[20]</sup> this work now demonstrates the first case of realizing the solvent-free processing of CDs materials in all three primary emissive colors.



This article is protected by copyright. All rights reserved.

**Figure 1. Schematic representation of prior and present work on CDs reshaping.** Previous work: inkjet printing with CDs solution; this work: solvent-free DIW with LCCDs.

## 2. Results and Discussion

To start with, CDs were first synthesized through a common solvothermal approach and then surface-modified through alkylation. As illustrated in **Figure 2a**, CDs with blue, green and red color emissions, respectively, were yielded when heating the mixture of citric acid monohydrate and *o*-phenylenediamine to 200 °C in sealed Teflon-lined autoclaves. Trial-and-error experiments based on our previous work showed that reasonable product yields could be achieved after 11 h reaction.<sup>[8a]</sup> Blue and green color emissive CDs, that are referred to as B- and G-CDs, respectively, were simultaneously produced with ethanol (EtOH) as the reaction medium, and subsequently collected after purification via silica gel column chromatography (Supporting Information, SI). By contrast, red color emissive CDs (R-CDs) were yielded while using the mixture of H<sub>2</sub>O and *N,N*-dimethylformamide (DMF) as the reaction medium. Alkylation has been proven facile to implement liquid crystallization,<sup>[21]</sup> which was exerted here in DMF via nucleophilic substitution of bromoalkanes (C<sub>n</sub>H<sub>2n+1</sub>Br, n = 10, 14, 16, 18 and 22, respectively) by the amino and/or hydroxyl groups on the CDs surface. LCCDs were produced after 40 h reaction at 90 °C and finally collected with purification through silica gel column chromatography. Excitingly, the surface alkylation

This article is protected by copyright. All rights reserved.

substantially depressed the common ACQ effect of CDs and afforded bright emissions in the bulk material form. The absolute fluorescence quantum yields (QY) were measured to be 69%, 2% and 31% for the blue, green and red emissive LCCDs, that are referred to as B-, G- and R-LCCDs, respectively (**Figure 2c**). In sharp contrast, the QY was measured to be effectively zero for B- and G-CDs and 1% for R-CDs before surface modification (**Figure 2b**).

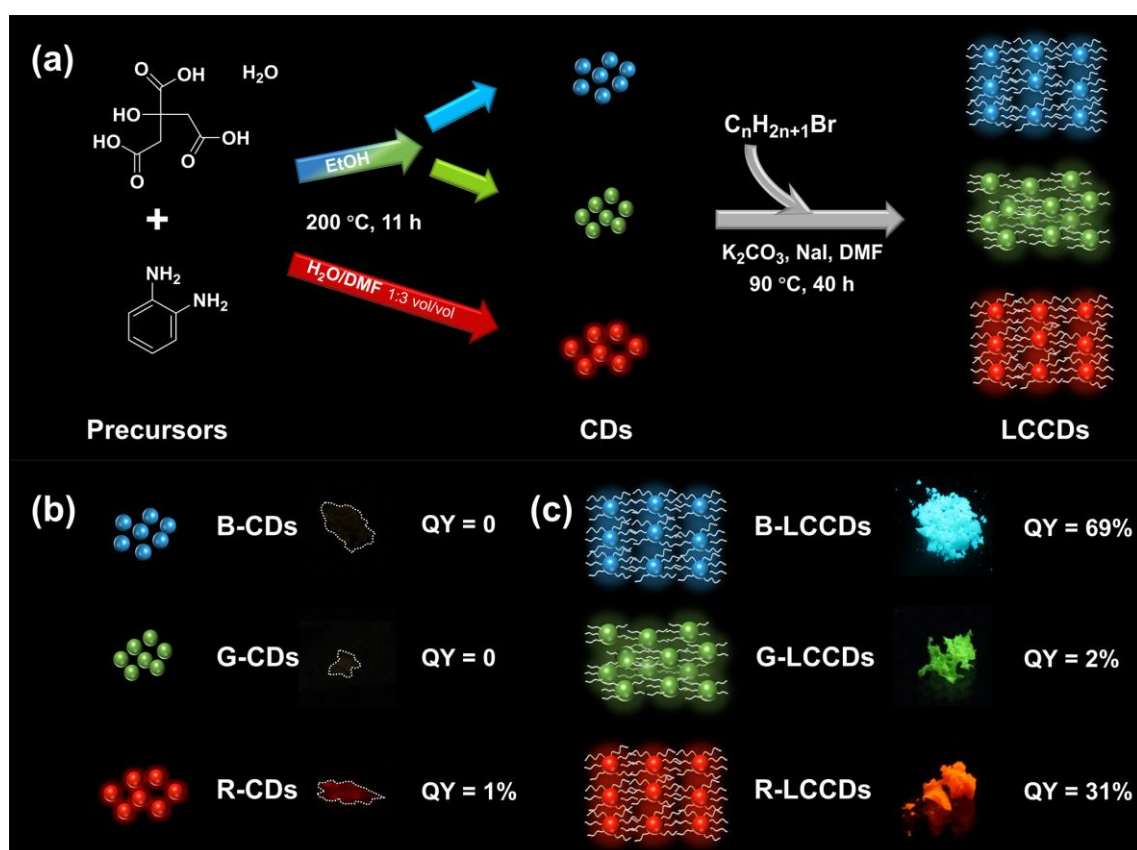


**Figure 2. Boosted fluorescence in bulk via liquid crystallization of CDs.** (a) Schematic diagram of the synthesis of CDs and LCCDs with varying fluorescence colors. (b) Photographs and fluorescence

quantum yields (QY) of B-, G- and R-CDs in bulk under 365 nm UV light. (c) Photographs and fluorescence QY of LCCDs in bulk under 365 nm UV light.

The surface alkylation of CDs by reacting with 1-bromohexadecane ( $C_nH_{2n+1}Br$ ,  $n = 16$ ) was first studied as hexadecyl groups were proven effective to impart LC functions to metal complexes in our previous work.<sup>[21]</sup> The study was comprehensively conducted by high-resolution transmission electron microscopy (HR-TEM), proton nuclear magnetic resonance spectroscopy ( $^1H$  NMR), Fourier transform infrared spectroscopy (FT-IR) and thermogravimetric analysis (TGA). TEM images show that the nanoparticles of B-, G- and R-CDs had diameters of  $1.3\pm 0.3$ ,  $2.9\pm 0.3$  and  $2.2\pm 0.4$  nm, respectively (**Figure 3a, 3f, 3k** and **S1**). The nanoparticle diameter was significantly increased to  $2.7\pm 0.3$ ,  $3.7\pm 0.7$  and  $2.7\pm 0.3$  nm for the B-, G- and R-LCCDs- $n$  ( $n = 16$ ), respectively (**Figure 3b, 3g, 3l** and **S1**). The increase of nanoparticle size was ascribed to the chemical bonding of hexadecyl chains on the CDs surface with a grafting density of 11, 1, or 3 pcs·nm<sup>-2</sup> for the B-, G- or R-LCCDs-16, respectively, according to the TGA results (**Table S1** and **Figure S2**). Notably, the graphene-like structures were maintained during surface alkylation, confirmed by the well-resolved lattice fringes in a spacing of 0.21 nm under HR-TEM. This tiny spacing indexed to the (100) lattice plane was given by the graphitic carbons.<sup>[22]</sup>  $^1H$  NMR results further verify the success of surface alkylation with hexadecyl chains. As displayed in **Figure 3c**, chemical shifts at 4.05 and 3.64 ppm are clear for the purified B-LCCDs-16, which can be assigned to the

This article is protected by copyright. All rights reserved.

Accepted Article

methylene groups directly linked to the oxygen and nitrogen atoms, respectively.<sup>[23]</sup> Chemical shifts peaked in the range of 0.86~1.59 ppm were also given by the methyl and other methylene groups, indicative of successful alkylation on the B-CDs surface. The amount of primary amine substitution is 8 times that of oxygen substitution during surface alkylation according to the NMR integration. Similar <sup>1</sup>H NMR results are given by the purified R-LCCDs-16 despite the fact that the amount of primary amine substitution is just 2.5 times that of oxygen substitution (**Figure 3m**). By contrast, only primary amine substitution is observed in the purified G-LCCDs-16 and the adjacent methylene group displays a chemical shift at 3.52 ppm (**Figure 3h**). The <sup>1</sup>H NMR results imply that an increase in the CDs size is unfavorable for surface alkylation, which is reasonable due to the declined specific area and active groups on the surface. FT-IR spectra can provide complementary information about the surface alkylation. As shown in **Figure 3d**, 3396, 3359 and 3189 cm<sup>-1</sup> bands are clear for B-CDs ascribed to the bending and stretching vibration of the primary amine, and the stretching vibration of hydroxyl groups, respectively.<sup>[18a,24]</sup> After alkylation, the primary amine is converted to secondary amine, giving a stretching vibration band at 3329 cm<sup>-1</sup> in the resulting B-LCCDs-16. In addition, compared with that in B-CDs, the hydroxyl vibration band moves to 3232 cm<sup>-1</sup> with an augmentation of 43 cm<sup>-1</sup> due to the significantly weakened hydrogen bonding interactions.<sup>[25]</sup> Similar FT-IR spectra changes occurred when converting R-CDs to R-LCCDs-16 (**Figure 3n**). In sharp contrast, the blueshift of hydroxyl vibration

This article is protected by copyright. All rights reserved.

peak is much smaller (only  $5\text{ cm}^{-1}$ ) when converting G-CDs to G-LCCDs-16 due to negligible oxygen substitution (**Figure 3i**), which is consistent with the  $^1\text{H}$  NMR results. Compared with such results for B- and R-LCCDs-16, the smaller shift of the amino vibration band might be ascribed to the much smaller grafting ratio as aforementioned. Interestingly, primary emissions in blue, green and red colors were maintained after surface alkylation. The resulting B-, G- and R-LCCDs-16 in ethanol displayed peak emissions at 473, 550 and 608 nm with absolute QY of 90%, 26% and 27%, respectively (**Figure 3e, 3j, 3o**).

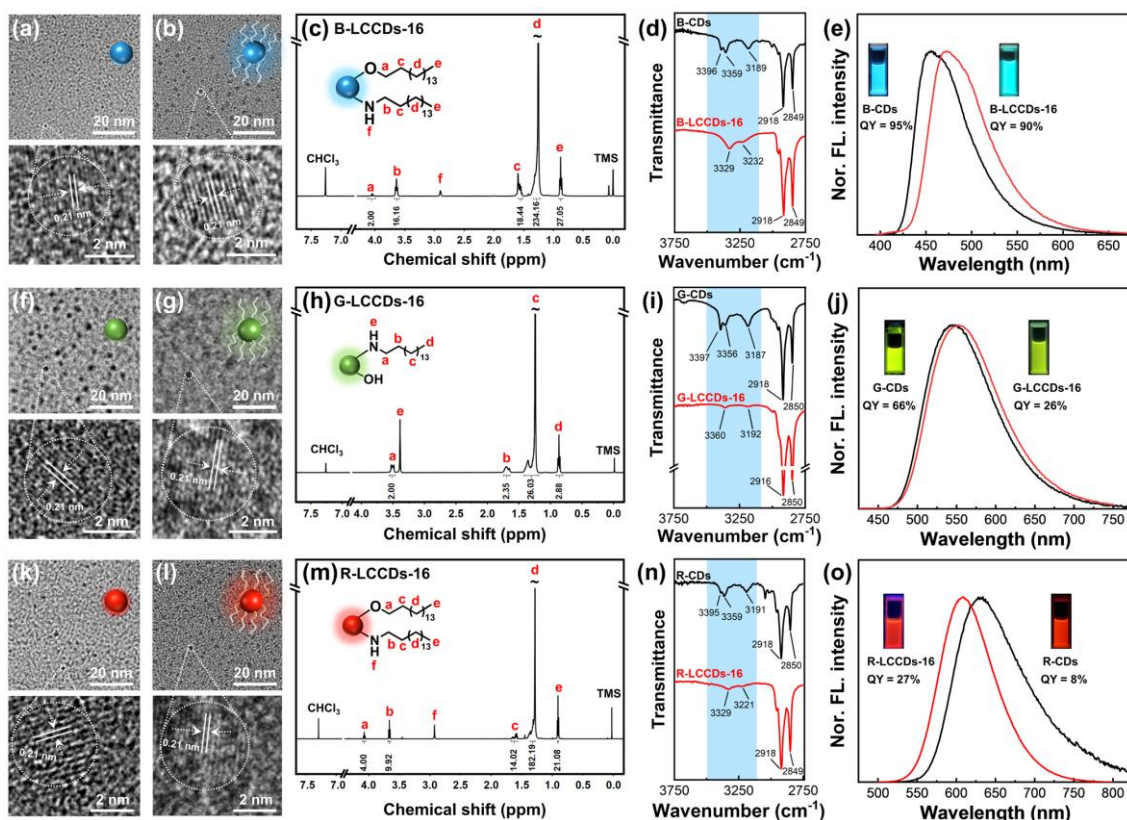


**Figure 3. Surface decoration of CDs with hexadecyl groups.** TEM images: (a) B-CDs, (b) B-LCCDs-16, (f) G-CDs, (g) G-LCCDs-16, (k) R-CDs, (l) R-LCCDs-16. Bottom: HR-TEM images.  $^1\text{H}$

This article is protected by copyright. All rights reserved.

NMR spectra: (c) B-LCCDs-16, (h) G-LCCDs-16, (m) R-LCCDs-16. FT-IR spectra: (d) B-CDs (top) and B-LCCDs-16 (bottom), (i) G-CDs (top) and G-LCCDs-16 (bottom), (n) R-CDs (top) and R-LCCDs-16 (bottom). Fluorescence spectra and QY in EtOH: (e) B-CDs and B-LCCDs-16, (j) G-CDs and G-LCCDs-16, (o) R-CDs and R-LCCDs-16. Nor. FL. intensity means normalized fluorescence intensity.

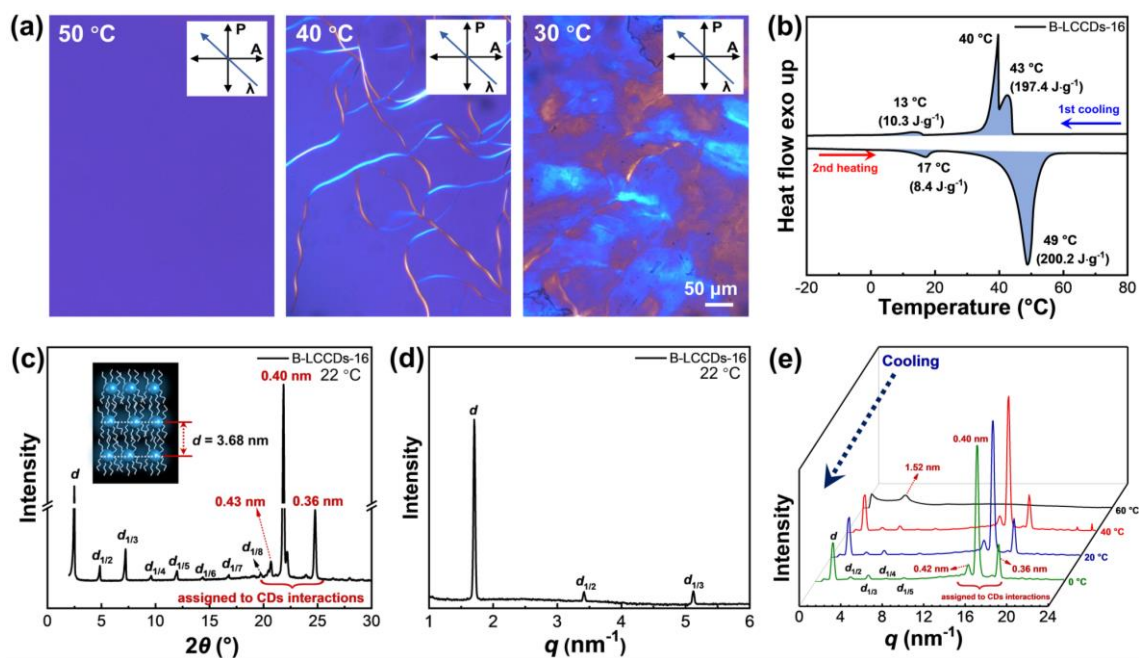
LCCDs in smectic phases were achieved by surface alkylation of CDs with hexadecyl chains. The identification of the LC phases was performed by the combination of polarized optical microscopy (POM), differential scanning calorimetry (DSC), wide-angle X-ray diffraction (WAXD), small-angle X-ray scattering (SAXS) and temperature-related wide-angle X-ray scattering (T-WAXS). For the as-prepared B-LCCDs-16, no birefringence can be observed at 50 °C, indicative of an isotropic phase (**Figure 4a**). In sharp contrast, B-CDs are crystalline even at a high temperature of 200 °C (**Figure S3**), indicating a significant decrease of phase transition temperature by surface alkylation. Upon cooling to a temperature near 40 °C, the resulting B-LCCDs-16 give string-like birefringent textures with bright blue and copper rose colors, respectively, suggesting an isotropic-mesophase transition and LC ordering.<sup>[26]</sup> When further lowering down the temperature to 30 °C, the textures start to exhibit birefringent patterns with focal conics, implying changes of phase retardation associated with a molecular rearrangement. Analyzing the thermal properties with DSC reveals large exothermic peaks at 43 and 40 °C upon cooling, respectively (**Figure 4b**), which are ascribed to the isotropic-mesophase transition and a further improvement of self-assembly

This article is protected by copyright. All rights reserved.

ordering, respectively. The improvement of self-assembly ordering can be verified by T-WAXS profiles as shown in **Figure S4**. Notably, a much smaller exothermic peak is also observed at 13 °C upon cooling due to the hexadecyl chain packing,<sup>[21]</sup> which is verified by the crystallization induced exothermic peak at 15 °C for *n*-hexadecane (**Figure S5**). Compared with the more than two times larger enthalpy observed in the LC platinum complexes,<sup>[21]</sup> the small enthalpy of 10.3 J·g<sup>-1</sup> detected here implies a constrained movement of hexadecyl chains by the CDs core. Basically, these phase transitions are reversible upon heating despite slight variations of the temperature and enthalpy. The self-assembly structure of B-LCCDs-16 is found to be highly ordered smectic at room temperature according to WAXD. As illustrated in **Figure 4c**, a consecutive sequence of diffraction peaks are clear at  $2\theta$  values of 2.4°, 4.8°, 7.2°, 9.6°, 12.0°, 14.4°, 16.8°, 19.8°, respectively, giving a reciprocal *d*-spacing ratio of 1:2:3:4:5:6:7:8 according to the Bragg law,  $m\lambda = 2d \sin \theta$ .<sup>[27]</sup> Where *m* stands for the diffraction order equaling 1 to 8, respectively, and *d* signifies the lattice spacing in a value of 3.68 nm. Given the diameter of 2.7±0.3 nm of B-LCCDs-16, the smectic LC phase emerges from the spontaneous close stacking of B-LCCDs-16, which might be driven by the interactions of CDs as verified by the diffraction peaks at a  $2\theta$  value of 20°~25°. To be noted, the diffraction peaks with a spacing of 0.36 nm does not account for B-LCCDs-16 stacking but presumably for vertical  $\pi$ - $\pi$  stacking of graphene-like planes inside the CDs core. The room temperature SAXS pattern further confirms layered stacking of B-LCCDs-16 into

This article is protected by copyright. All rights reserved.

the smectic phase with a lattice spacing of 3.69 nm (**Figure 4d**), which has a good agreement with the WAXD results. T-WAXS profiles show that the layered stacking of B-LCCDs-16 can be disassembled upon heating. As displayed in **Figure 4e**, all smectic diffraction peaks are significantly decrease at 60 °C, and a broad halo is maintained at the  $q$  (the magnitude of scattering vector) of 4.1 nm<sup>-1</sup>. This  $q$  value suggests  $\pi$ - $\pi$  stacking of four graphene-like planes inside the CDs core with a total  $d$ -spacing of 1.52 nm. Upon cooling, diffraction peaks come back. Under temperatures below 40 °C, the  $q$  values are at 1.7, 3.4, 5.1, 6.8, 8.5 nm<sup>-1</sup>, respectively, giving a ratio of 1:2:3:4:5, and can be indexed to the smectic LC phase. Meanwhile, the 14.6~17.6 nm<sup>-1</sup> diffraction peaks are indicative of interactions belonged to CDs, respectively.



This article is protected by copyright. All rights reserved.

**Figure 4. Phase behaviors of B-LCCDs-16.** (a) POM images when cooling down from the isotropic state; P stands for “polarizer”, A marks “analyzer” and  $\lambda$  denotes “phase retarder”. (b) DSC curves. (c) WAXD pattern at 22 °C, inset: schematic of smectic phase arising from self-assembly. (d) SAXS pattern at 22 °C. (e) T-WAXS profiles during first cooling from 60 to 0 °C.

Room temperature highly ordered smectic phase is also observed in R-LCCDs-16. As shown in **Figure 5a**, no birefringence can be seen at 50 °C in the POM image, also indicative of isotropic phase. However, focal conic textures are clear when cooling down to 25 °C, suggesting the formation of smectic LC phases. DSC curves reveal that the isotropic-mesophase transition temperature peaks at 33 °C upon cooling, which changes to 40 °C during heating. The phase transition is also dramatic with a large enthalpy of 82.5~83.1 J·g<sup>-1</sup> (**Figure 5b**). The exothermic peak at 16 °C upon cooling and endothermic peak at 18 °C upon heating correspond to the crystallization and melting of hexadecyl chains, respectively. Compared with the case in B-LCCDs-16, the more than 3 times higher enthalpy (31.8~32.9 J·g<sup>-1</sup>) implies smaller confinement of the alkyl chain movement by the R-CDs core. The WAXD pattern at room temperature reveals a smectic stacking of R-LCCDs-16 with a *d*-spacing of 3.69 nm (**Figure 5c**), which is same as that of B-LCCDs-16. This could be anticipated given the identical nanoparticle diameter of 2.7±0.3 nm for the B- and R-LCCDs-16. T-WAXS profiles have confirmed the smectic LC phase below 30 °C (**Figure 5d**), which is driven by the interactions of CDs under the action of supramolecular van der Waals forces.

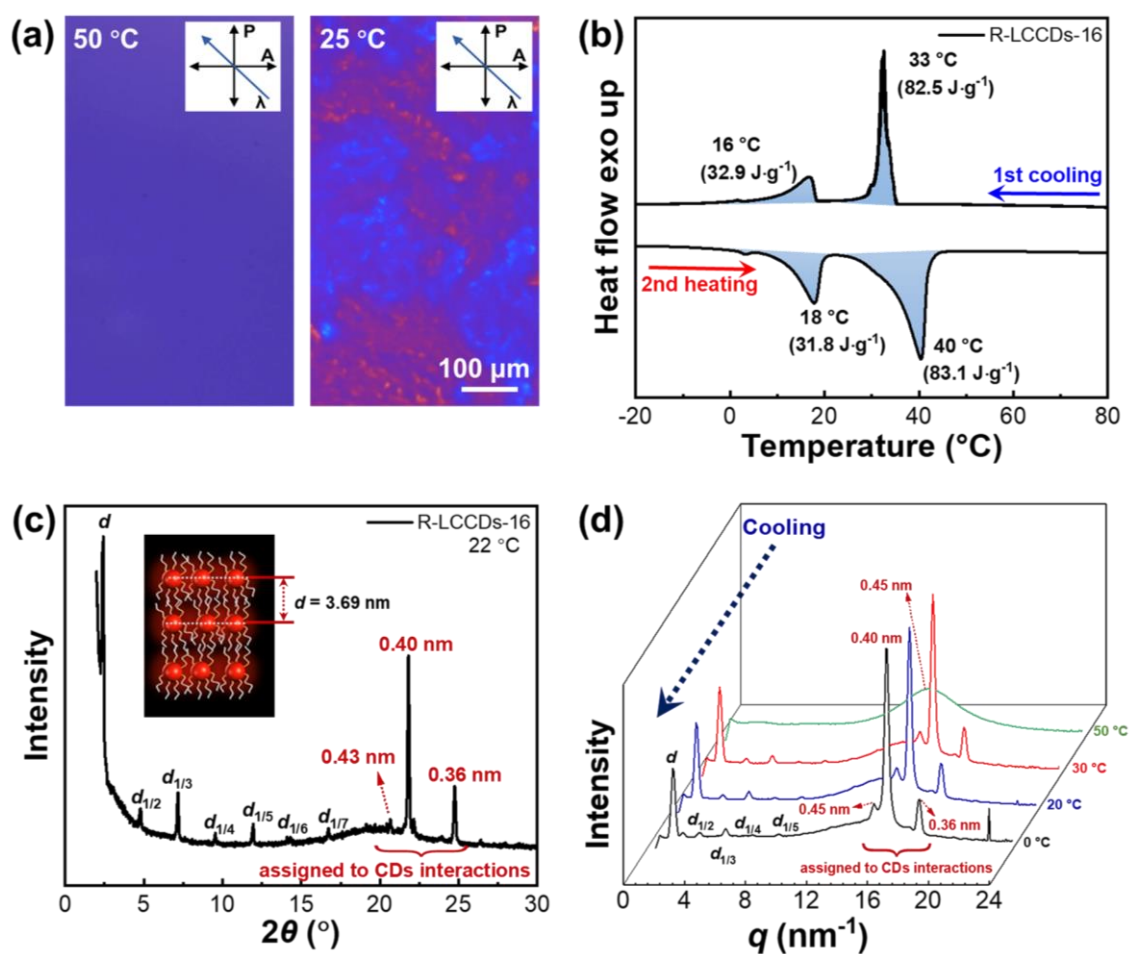


**Figure 5. Phase behaviors of R-LCCDs-16.** (a) POM images, and (b) DSC curves when cooling down from the isotropic state. (c) WAXD pattern at 22 °C; inset: schematic of the smectic phase emerging from the self-assembly. (d) T-WAXS profiles during first cooling.

Unfortunately, G-LCCDs-16 exhibit the crystalline phase rather than LC phase at room temperature, which would prevent or cause the difficulty in solvent-free processing. As shown in **Figure S6**, the isotropic-mesophase transition of G-LCCDs-16 occurs at a high temperature of 147 °C upon cooling, while the crystallization takes place at 53 °C, according to the quantitative analysis with POM, DSC, WAXD and T-WAXS. Even worse, in

This article is protected by copyright. All rights reserved.

comparison with the fluorescence in EtOH, bulk G-LCCDs-16 fluoresce yellow color rather than the predesigned green color at room temperature, as illustrated by the extremely large redshift of the emission peak from 550 to 625 nm. The unsatisfactory performance of G-LCCDs-16 forces us to further dial the phase behaviors of G-LCCDs.

Excitingly, the room temperature smectic LC phase can be achieved by varying the alkyl chain length on the G-CDs surface. Analyzing the  $^1\text{H}$  NMR spectra reveals that primary amine substitutions mainly account for the surface alkylation despite the variation of alkyl chain length ( $\text{C}_n\text{H}_{2n+1}$ ,  $n = 10, 14, 18, 22$ , respectively, **Figure S7**), as observed in G-LCCDs-16. A significant decrease of the crystallization temperature from 80 to  $-8$  °C is observed for G-LCCDs- $n$  by shortening the alkyl chain length (**Figure 6a, S8~S10**), which is mainly caused by the decreased crystallization temperature of the shorter alkyl chains (**Figure S5**). By contrast, the isotropic-mesophase transition temperature (i.e., the clearing point,  $T_c$ ) upon cooling first increases and then decreases with the decrease of  $n$ , which is found to be 104, 105, 147, 128 and 92 °C when  $n$  equals 22, 18, 16, 14 and 10, respectively. This may be attributed to the effects of both flexibility and intermolecular interactions. The chain flexibility and G-LCCDs- $n$  mobility can be decreased when shortening alkyl chains, leading to an increase of  $T_c$ . However, the intermolecular interactions are also decreased at the same time, which can prompt a decrease of  $T_c$ . Given G-LCCDs-10 can provide a low crystallization temperature at  $-8$  °C and a relatively high clearing point at 92 °C, the LC

This article is protected by copyright. All rights reserved.

phase can be maintained in a broad temperature range, which would benefit facile LC processing. TEM images show a small nanoparticle size of  $3.4\pm 0.7$  nm for the G-LCCDs-10 (**Figure S11**) and the nanoparticle core is in the form of vertically stacked graphene-like planes with a lateral lattice parameter of 0.21 nm (**Figure 6b**). The vertical  $\pi$ - $\pi$  stacking in a  $d$ -spacing of 0.36 nm is evidenced by the HR-TEM (**Figure S12**) and further confirmed by the WAXD peak at the  $2\theta$  of  $24.5^\circ$  (**Figure 6c**). The highly ordered smectic LC phase is also confirmed by the consecutive sequence of WAXD peaks that give a reciprocal  $d$ -spacing ratio of 1:2:3:4:5:6:7. The parameters in spacing of 0.49 and 0.41 nm are also detected, which perhaps belong to the CDs stacking and as the same with B-LCCDs-16 and R-LCCDs-16. POM images show that no birefringence can be observed at 100 °C for G-LCCDs-10, and the isotropic-mesophase transition can occur when the temperature is lower than 90 °C with the formation of focal conic textures (**Figure 6d**). DSC curves imply complicated phase transition behaviors of G-LCCDs-10. As displayed in **Figure 6e**, upon cooling four exothermic peaks are given at 92, 26, 17 and  $-8$  °C, which turn to endothermic peaks at 96, 57, 32 and 13 °C during heating, respectively. The first group of thermic peaks are led by the reversible isotropic-mesophase transition, and the last group of thermic peaks are ascribed to the crystallization and crystalline-mesophase transition of G-LCCDs-10, respectively. However, the second and third groups of thermic peaks are difficult to understand. To provide a deeper and reliable understanding, T-WAXS analysis was exerted. Results show

This article is protected by copyright. All rights reserved.

that there are two groups of layered stacking for G-LCCDs-10 at 70 °C, with a lattice parameter of 1.92 nm for one and 1.72 nm for another (**Figure 6f**). Considering the nanoparticle diameter of  $3.4\pm 0.7$  nm that is much larger than the lattice parameter (1.92 or 1.72 nm), intercalated structures are believed to form by G-LCCDs-10.<sup>[28]</sup> Upon cooling to 40 °C, the diffraction peaks at the  $q$  value of 2.5 and 2.9 nm<sup>-1</sup> represent an increase of  $d$ -spacings to 2.51 and 2.17 nm, respectively (**Figure 6g** and **S13**). The increase of lattice spacing might be due to the significantly reduced mobility of the decyl chains, and the short alkyl chains may perform as “rigid” rods. The diffraction peaks in the range of 0~24.0 nm<sup>-1</sup> can be divided into two groups which obey the (00*l*) or (00*l*') rule, in which the peaks unmarked in the pattern are assigned to the retained structure at 70 °C (**Figure S13a**). A little decrease of  $d$ -spacings to 2.45 and 2.13 nm, respectively, are observed for  $d$  and  $d'$  in **Figure S13b** that correspond to (001) and (001') facets when further lowering down the temperature to 20 °C. The other peaks also obey the (00*l*) or (00*l*') rule or are retained from higher temperatures. In conclusion, G-LCCDs-10 exhibit the intercalated smectic LC phase in the range of -8~92 °C (**Figure 6h**), and the increase of lattice spacing upon cooling in the temperature range accounts for higher-order transitions in the smectic phase.

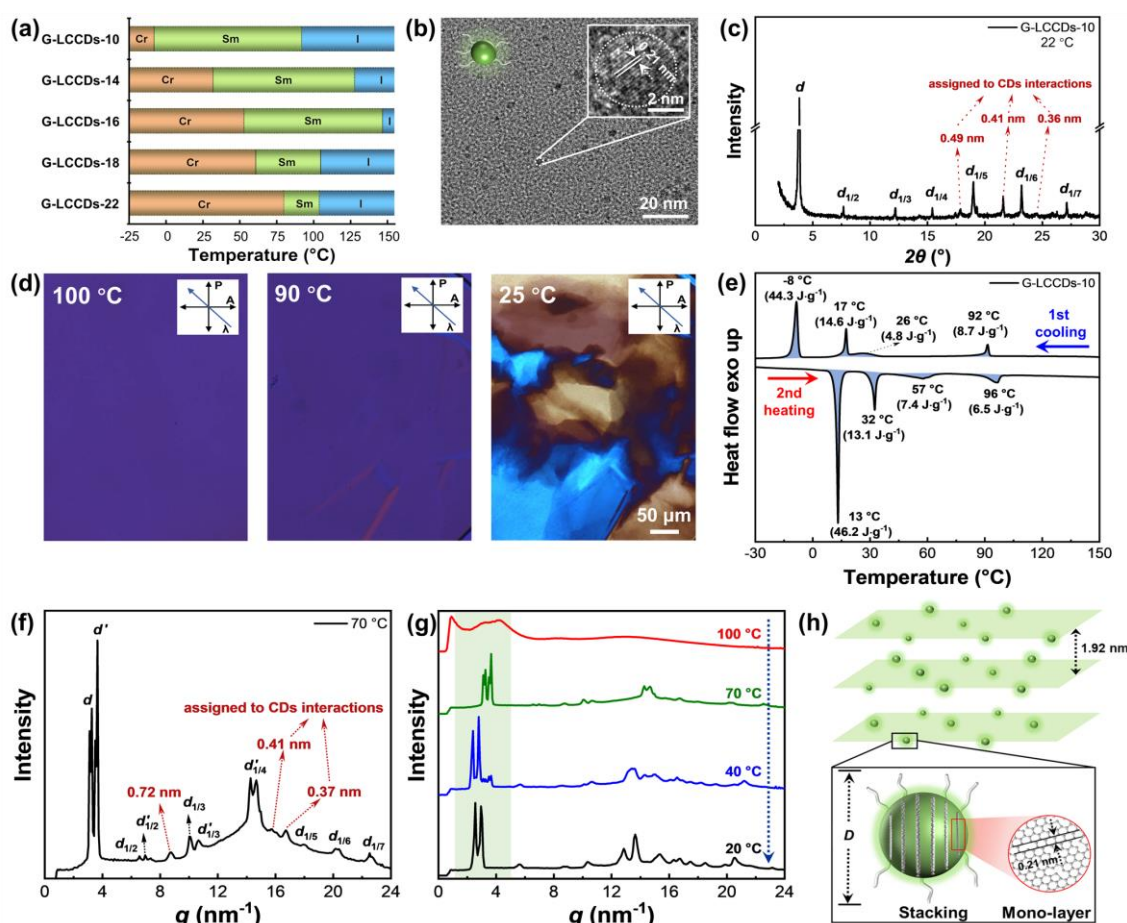


**Figure 6. Phase behaviors of G-LCCDs.** (a) Phase transition temperatures of G-LCCDs-*n* on the first cooling scan, wherein *n* represents the number of carbons in the alkyl chains (*n* = 10, 14, 16, 18, 22, respectively). (b) TEM and HR-TEM images (inset) of G-LCCDs-10. (c) WAXD pattern of G-LCCDs-10 at 22 °C. (d) POM images of G-LCCDs-10 when cooling down from the isotropic state. (e) DSC curves of G-LCCDs-10. (f) T-WAXS profile of G-LCCDs-10 at 70 °C. (g) T-WAXS profiles of G-LCCDs-10 when cooling down from 100 to 20 °C. (h) Schematic diagram of the intercalated smectic phase of G-LCCDs-10.

The prepared B-LCCDs-16, G-LCCDs-10 and R-LCCDs-16 are not only able to produce bright emissions at room temperature, but can also enable solvent-free processing in

This article is protected by copyright. All rights reserved.

their mesophase. As shown in **Figure 7a~c**, upon excitation by 365 nm UV light, bulk B-LCCDs-16, G-LCCDs-10 and R-LCCDs-16 give peak emissions at 475, 523 and 607 nm, with QY of 69%, 2% and 31%, respectively. The color purity of the fluorescence images may be smaller than expected due to the relatively large full width at half maximum (FWHM) of the fluorescence spectra.<sup>[4e,29]</sup> These brightly emissive LCCDs appear as waxy solid at room temperature, while becoming liquid at the temperature higher than  $T_c$  (**Figure 7d~f**). Rheological measurements show that the viscosity of both R-LCCDs-16 and B-LCCDs-16 is dramatically reduced upon heating while that of G-LCCDs-10 first decreases, then increases and finally decreases (**Figure S14**). Basically, the internal friction is reduced upon heating and thus gives rise to viscosity reduction. The unexpected increase of viscosity from 12 to 219 Pa·s when heating G-LCCDs-10 from 40 to 70 °C may be due to the increased friction by the decrease of  $d$ -spacing in the smectic phase as discussed in the previous paragraph. The temperature-dependent viscosity is promising for facile extrusion-based printing without the use of solvents, where a low viscosity is useful for processing while the high viscosity is required to maintain the printed objects. Herein, we demonstrate the example of solvent-free DIW of these designed LCCDs (**Figure 8a**). The DIW was successfully exerted using a home-made setup consisting of a syringe pump, a 25  $\mu$ L syringe with needle head and a temperature controller (**Figure 8b**). Two main parameters were carefully controlled for precise processing, e.g., the extrusion speed (10 mm/min) and syringe temperature ( $T$ ).

This article is protected by copyright. All rights reserved.

Excitingly, a good DIW fidelity was achieved in the LC phase ( $T < T_c$ , **Figure 8c**). In sharp contrast, the geometrical accuracy is far beyond controlled when exerting DIW in the isotropic phase ( $T > T_c$ ). The improvement resolution seen in the LC phase is likely due to the formation of a more orderly molecular alignment that is led by stronger supramolecular van der Waals interactions. Good geometrical accuracy can be enabled with a line width of 222, 205 and 176  $\mu\text{m}$  for the brightly emissive B-LCCDs-16, G-LCCDs-10 and R-LCCDs-16, respectively (**Figure 8d**), despite slightly larger than the needle diameter (150  $\mu\text{m}$ ) due to the die-swell effect. Better printing resolution may be achieved by future optimization of the home-made setup and materials that we used.

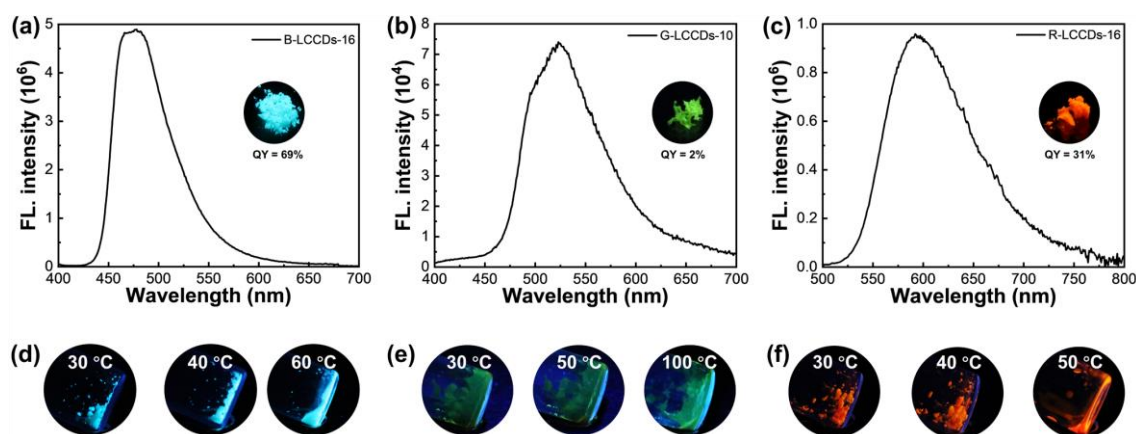


**Figure 7. Fluorescence and thermoresponsive behaviors of LCCDs.** Fluorescence (FL.) spectra in bulk: (a) B-LCCDs-16, (b) G-LCCDs-10, (c) R-LCCDs-16. Insets: Photographs under a hand-held 365 nm UV lamp and the corresponding QY. Temperature-dependent flow behaviors of (d) B-LCCDs-16, (e) G-LCCDs-10, and (f) R-LCCDs-16.

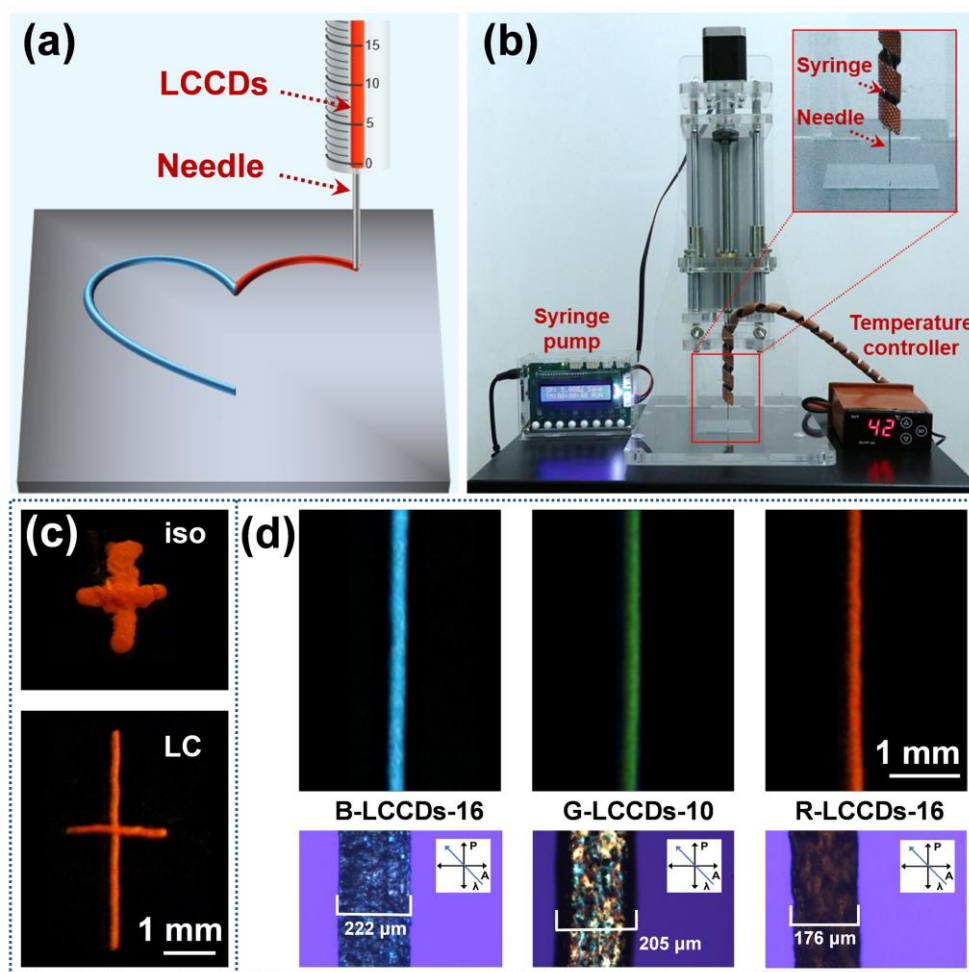


**Figure 8. DIW with LCCDs.** (a) Scheme showing the solvent-free DIW of LCCDs. (b) Photograph of the home-made DIW setup. (c) Comparison of DIW in the isotropic (iso) phase and in the LC phase. (d) Top: fluorescent lines printed with LCCDs; bottom: the magnified POM images. DIW temperature: red, 30 °C; blue, 40 °C; green, 30 °C.

### 3. Conclusions

This article is protected by copyright. All rights reserved.

In summary, we have demonstrated the first example of solvent-free DIW of CDs via liquid crystallization. This liquid crystallization was implemented by pre-designed grafting flexible alkyl chains on the CDs surface. The successful grafting was confirmed by TEM,  $^1\text{H}$  NMR and FT-IR, and the resulting LCCDs in smectic phase were identified by the combination of DSC, POM, WAXD, SAXS and T-WAXS. Results indicate that the formulated LCCDs displayed varying phase transition behaviors depending on the number of carbons in the alkyl chains (e.g.,  $n = 10, 14, 16, 18$  and  $22$ , respectively). With  $n$  equaling  $16, 10$  and  $16$ , respectively, viscoelastic inks with blue, green and red color emissions were separately achieved for low temperature ( $< 50\text{ }^\circ\text{C}$ ) DIW. Eventually, bright colored fluorescent lines were successfully printed via solvent-free DIW. Wherein, interactions of alkyl chains and CDs led by supramolecular van der Waals forces played a critical role, which not only endowed self-supporting properties to the printed objects, but also depressed the common ACQ effect. Unexpectedly, compared with DIW in the isotropic phase, the spatial resolution was significantly improved in the LC phase. The reported paradigm can not only display a significant fundamental advance in terms of imparting LC properties (e.g., long-range orientational order, facile reversible thermoresponse) to CDs, but also promises DIW based advanced manufacturing with CDs toward high-tech applications despite better printing resolution and the printability for 3D architectures need to be further tuned via optimization of printing setups and materials. The DIW method based on LCCDs

This article is protected by copyright. All rights reserved.

demonstrated in this work opens a platform for solvent-free printing of security tags by taking advantage of the well-controlled and easily recognizable fluorescence emission and LC characteristics. Enormous potential applications are worth exploring in electronics, soft robotics, actuators and so on in the future.

### **Supporting information**

Supporting information is available from the Wiley Online Library or from the author.

### **Conflicts of interest**

The authors declare that there are no conflicts of interest.

### **Acknowledgments**

The authors gratefully appreciate the funds from the National Natural Science Foundation of China (52122316, 52073108, 52233005), and the Innovation and Talent Recruitment Base of New Energy Chemistry and Device (B21003). They also thank Assoc. Prof. Bijin Xiong from the School of Chemistry and Chemical Engineering in HUST for the SAXS tests assistances, technical assistances from the HUST Analytical and Testing Center, and Core Facilities of Life and Sciences. I.I.S. Acknowledges the hospitality of the

This article is protected by copyright. All rights reserved.

International Institute of HUST for Sustainability with Knotted Chiral Meta Matter (SKCM<sup>2</sup>) during his sabbatical stay, when this manuscript was being prepared for submission.

Received: ((will be filled in by the editorial staff))

Revised: ((will be filled in by the editorial staff))

Published online: ((will be filled in by the editorial staff))

## References

- [1] X. Lim, *Nature* **2016**, *531*, 26.
- [2] a) J. Yang, M. Fang, Z. Li, *Aggregate* **2020**, *1*, 6; b) G. Huang, Q. Xia, W. Huang, J. Tian, Z. He, B. S. Li, B. Z. Tang, *Angew. Chem. Int. Ed.* **2019**, *58*, 17814; c) S. Xu, Y. Duan, B. Liu, *Adv. Mater.* **2020**, *32*, 1903530; d) J. Ji, D. Hu, J. Yuan, Y. Wei, *Adv. Mater.* **2020**, *32*, 2004616; e) Y. Zhao, H. Peng, X. Zhou, Z. Li, X. Xie, *Adv. Sci.* **2022**, *9*, 2105903; f) Y. Zhao, X. Y. Zhao, M. D. Li, Z. A. Li, H. Y. Peng, X. L. Xie, *Angew. Chem. Int. Ed.* **2020**, *59*, 10066; g) R. Qu, X. Zhen, X. Jiang, *CCS Chem.* **2021**, *4*, 401; h) X. Yu, K. Liu, H. Zhang, B. Wang, G. Yang, J. Li, J. Yu, *CCS Chem.* **2021**, *3*, 252.
- [3] a) Y.-P. Sun, B. Zhou, Y. Lin, W. Wang, K. A. S. Fernando, P. Pathak, M. J. Meziani, B. A. Harruff, X. Wang, H. Wang, P. G. Luo, H. Yang, M. E. Kose, B. Chen, L. M. Veca, S.-Y. Xie, *J. Am. Chem. Soc.* **2006**, *128*, 7756; b) X. Xu, R. Ray, Y. Gu, H. Ploehn, L. Gearheart, K. Raker, W. Scrivens, *J. Am. Chem. Soc.* **2004**, *126*, 12736; c) H. Liu, T. Ye, C. Mao, *Angew. Chem. Int. Ed.* **2007**, *46*, 6473.

This article is protected by copyright. All rights reserved.

- [4] a) L. Ai, Z. Song, M. Nie, J. Yu, F. Liu, H. Song, B. Zhang, G. I. N. Waterhouse, S. Lu, *Angew. Chem. Int. Ed.* **2022**, e202217822; b) F. Yuan, Z. Wang, X. Li, Y. Li, Z. Tan, L. Fan, S. Yang, *Adv. Mater.* **2017**, *29*, 1604436; c) B. Wang, J. Yu, L. Sui, S. Zhu, Z. Tang, B. Yang, S. Lu, *Adv. Sci.* **2021**, *8*, 2001453; d) S. Lu, L. Sui, J. Liu, S. Zhu, A. Chen, M. Jin, B. Yang, *Adv. Mater.* **2017**, *29*, 1603443; e) J. Liu, Y. Geng, D. Li, H. Yao, Z. Huo, Y. Li, K. Zhang, S. Zhu, H. Wei, W. Xu, J. Jiang, B. Yang, *Adv. Mater.* **2020**, *32*, 1906641; f) Y. Xian, K. Li, *Adv. Mater.* **2022**, *34*, 2201031.
- [5] a) K. Jiang, S. Sun, L. Zhang, Y. Lu, A. Wu, C. Cai, H. Lin, *Angew. Chem. Int. Ed.* **2015**, *54*, 5360; b) C. Xia, S. Zhu, S.-T. Zhang, Q. Zeng, S. Tao, X. Tian, Y. Li, B. Yang, *ACS Appl. Mater. Interfaces* **2020**, *12*, 38593; c) D. Li, C. Liang, E. V. Ushakova, M. Sun, X. Huang, X. Zhang, P. Jing, S. J. Yoo, J.-G. Kim, E. Liu, W. Zhang, L. Jing, G. Xing, W. Zheng, Z. Tang, S. Qu, A. L. Rogach, *Small* **2019**, *15*, 1905050.
- [6] a) S. Qu, X. Wang, Q. Lu, X. Liu, L. Wang, *Angew. Chem. Int. Ed.* **2012**, *51*, 12215; b) L. Đorđević, F. Arcudi, M. Cacioppo, M. Prato, *Nat. Nanotechnol.* **2022**, *17*, 112; c) K. Jiang, Y. Wang, C. Cai, H. Lin, *Adv. Mater.* **2018**, *30*, 1800783.
- [7] a) S. Zhu, Q. Meng, L. Wang, J. Zhang, Y. Song, H. Jin, K. Zhang, H. Sun, H. Wang, B. Yang, *Angew. Chem. Int. Ed.* **2013**, *52*, 3953; b) A. Xu, G. Wang, Y. Li, H. Dong, S. Yang, P. He, G. Ding, *Small* **2020**, *16*, 2004621; c) M. Park, Y. Jeong, H. S. Kim, W. Lee, S.-H. Nam, S. Lee, H. Yoon, J. Kim, S. Yoo, S. Jeon, *Adv. Funct. Mater.* **2021**, *31*, 2102741; d) H. Yang, Y. Liu, Z. Guo, B. Lei, J. Zhuang, X. Zhang, Z. Liu, C. Hu, *Nat. Commun.* **2019**, *10*, 1789.
- [8] a) Y. Wang, X. Hao, H. Peng, X. Zhou, X. Xie, *Macromol. Rapid Commun.* **2022**, *43*, 2100868; b) K. Jiang, L. Zhang, J. Lu, C. Xu, C. Cai, H. Lin, *Angew. Chem. Int. Ed.*

This article is protected by copyright. All rights reserved.

- 2016, 55, 7231; c) J. Wang, C.-F. Wang, S. Chen, *Angew. Chem. Int. Ed.* **2012**, 51, 9297; d) J. Liu, N. Wang, Y. Yu, Y. Yan, H. Zhang, J. Li, J. Yu, *Sci. Adv.* **2017**, 3, e1603171.
- [9] K. Jin, J. Zhang, W. Tian, X. Ji, J. Yu, J. Zhang, *ACS Sustainable Chem. Eng.* **2020**, 8, 5937.
- [10] T. Liu, G. Yin, Z. Song, J. Yu, X. Yong, B. Zhang, L. Ai, S. Lu, *ACS Mater. Lett.* **2023**, 5, 846.
- [11] a) T. Geelhaar, K. Griesar, B. Reckmann, *Angew. Chem. Int. Ed.* **2013**, 52, 8798; b) S. Chai, F. Xu, R. Zhang, X. Wang, L. Zhai, X. Li, H.-J. Qian, L. Wu, H. Li, *J. Am. Chem. Soc.* **2021**, 143, 21433; c) H. Mandoor, B. Senyuk, I. I. Smalyukh, *Science* **2016**, 352, 69; d) K. G. Gutierrez-Cuevas, L. Wang, Z. Zheng, H. K. Bisoyi, G. Li, L.-S. Tan, R. A. Vaia, Q. Li, *Angew. Chem. Int. Ed.* **2016**, 55, 13090; e) Y. X. Hu, X. T. Hao, L. Xu, X. L. Xie, B. J. Xiong, Z. B. Hu, H. T. Sun, G. Q. Yin, X. P. Li, H. Y. Peng, H. B. Yang, *J. Am. Chem. Soc.* **2020**, 142, 6285; f) Z. Yu, X. Wan, H. Tu, X. Chen, Q. Zhou., *Acta Polym. Sin.* **2003**, 430.
- [12] a) T. Kosa, L. Sukhomlinova, L. Su, B. Taheri, T. J. White, T. J. Bunning, *Nature* **2012**, 485, 347; b) M. del Pozo, J. A. H. P. Sol, A. P. H. J. Schenning, M. G. Debije, *Adv. Mater.* **2022**, 34, 2104390.
- [13] J. Zhang , C. Hou, T. Li , J. Jiang, W. F. Dong., *Acta Polym. Sin.* **2022**, 53, 1332.
- [14] H. Zhou, C. Xue, P. Weis, Y. Suzuki, S. Huang, K. Koynov, G. K. Auernhammer, R. Berger, H.-J. Butt, S. Wu, *Nat. Chem.* **2017**, 9, 145.

- [15] Y. Liu, S. Liang, C. Yuan, A. Best, M. Kappl, K. Koynov, H.-J. Butt, S. Wu, *Adv. Funct. Mater.* **2021**, *31*, 2103908.
- [16] S. J. D. Lugger, L. Ceamanos, D. J. Mulder, C. Sánchez-Somolinos, A. P. H. J. Schenning, *Adv. Mater. Technol.* **2022**, 2201472.
- [17] H. Peng, L. Yu, G. Chen, Z. Xue, Y. Liao, J. Zhu, X. Xie, I. I. Smalyukh, Y. Wei, *ACS Appl. Mater. Interfaces* **2019**, *11*, 8612.
- [18] a) M. A. S. R. Saadi, A. Maguire, N. T. Pottackal, M. S. H. Thakur, M. M. Ikram, A. J. Hart, P. M. Ajayan, M. M. Rahman, *Adv. Mater.* **2022**, *34*, 2108855; b) S.-J. Yuan, W.-H. Meng, A.-H. Du, X.-Y. Cao, Y. Zhao, J.-X. Wang, L. Jiang, *Chin. J. Polym. Sci.* **2019**, *37*, 729.
- [19] a) Y. Guo, H. Shahsavan, M. Sitti, *Adv. Mater.* **2020**, *32*, 2002753; b) X. Peng, S. Wu, X. Sun, L. Yue, S. M. Montgomery, F. Demoly, K. Zhou, R. R. Zhao, H. J. Qi, *Adv. Mater.* **2022**, *34*, 2204890; c) J. A. H. P. Sol, H. Sentjens, L. Yang, N. Grossiord, A. P. H. J. Schenning, M. G. Debije, *Adv. Mater.* **2021**, *33*, 2103309; d) J. A. H. P. Sol, L. G. Smits, A. P. H. J. Schenning, M. G. Debije, *Adv. Funct. Mater.* **2022**, *32*, 2201766.
- [20] Q. Yang, J.-C. Zhu, Z.-X. Li, X.-S. Chen, Y.-X. Jiang, Z.-W. Luo, P. Wang, H.-L. Xie, *ACS Appl. Mater. Interfaces* **2021**, *13*, 26522.
- [21] X. Hao, B. Xiong, M. Ni, B. Tang, Y. Ma, H. Peng, X. Zhou, I. I. Smalyukh, X. Xie, *ACS Appl. Mater. Interfaces* **2020**, *12*, 53058.
- [22] Y. Dong, H. Pang, H. B. Yang, C. Guo, J. Shao, Y. Chi, C. M. Li, T. Yu, *Angew. Chem. Int. Ed.* **2013**, *52*, 7800.
- [23] J. L. Sudmeier, C. N. Reilley, *Anal. Chem.* **1964**, *36*, 1698.

This article is protected by copyright. All rights reserved.

- [24] L. Đorđević, F. Arcudi, A. D'Urso, M. Cacioppo, N. Micali, T. Bürgi, R. Purrello, M. Prato, *Nat. Commun.* **2018**, *9*, 3442.
- [25] a) Z. Zhou, W. Wei, S. Li, Y. Zhang, Q. Yao, M. Ni, H. Peng, X. Zhou, X. Xie, *ACS Sustainable Chem. Eng.* **2021**, *9*, 5902; b) G. Chen, W. Wei, S. Li, X. Zhou, Z. Li, H. Peng, X. Xie, *Mater. Chem. Front.* **2022**, *6*, 3531.
- [26] M.-J. Gim, D. A. Beller, D. K. Yoon, *Nat. Commun.* **2017**, *8*, 15453.
- [27] a) M. del Pozo, L. Liu, M. Pilz da Cunha, D. J. Broer, A. P. H. J. Schenning, *Adv. Funct. Mater.* **2020**, *30*, 2005560; b) V. Krishnasamy, W. Qu, C. Chen, H. Huo, K. Ramanagul, V. Gothandapani, G. H. Mehl, Q. Zhang, F. Liu, *Macromolecules* **2020**, *53*, 4193.
- [28] C. T. Imrie, P. A. Henderson, *Curr. Opin. Colloid Interface Sci.* **2002**, *7*, 298.
- [29] a) D. Li, P. Jing, L. Sun, Y. An, X. Shan, X. Lu, D. Zhou, D. Han, D. Shen, Y. Zhai, S. Qu, R. Zbořil, A. L. Rogach, *Adv. Mater.* **2018**, *30*, 1705913; b) Q. Zhang, R. Wang, B. Feng, X. Zhong, K. Ostrikov, *Nat. Commun.* **2021**, *12*, 6856.

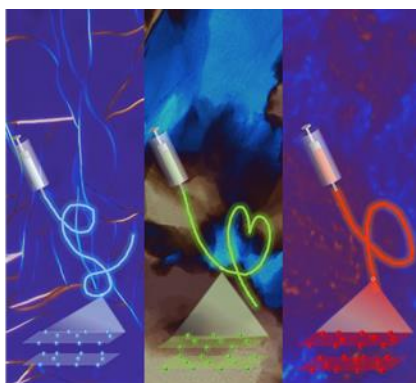
## Table of Contents

The first case of solvent-free direct ink writing (DIW) of carbon dots was demonstrated via liquid crystallization, giving rise to highly luminescent fluorescent patterns in three primary colors of blue, green and red, respectively, due to the significantly limited ACQ effect, and promising technological utility in DIW-based advanced manufacturing.

This article is protected by copyright. All rights reserved.

*Yixuan Wang, Yun Liu, Xingtian Hao, Xingping Zhou, Haiyan Peng,\* Zhihao Shen, Ivan I. Smalyukh, Xiaolin Xie,\* Bai Yang*

## Supramolecular Liquid Crystal Carbon Dots for Solvent-free Direct Ink Writing



This article is protected by copyright. All rights reserved.